NANO LETTERS

pubs.acs.org/NanoLett Letter

Three-Dimensional Perovskite Nanopixels for Ultrahigh-Resolution Color Displays and Multilevel Anticounterfeiting

Mojun Chen, Shiqi Hu, Zhiwen Zhou, Nan Huang, Sanghyeon Lee, Yage Zhang, Rui Cheng, Jihyuk Yang, Zhaoyi Xu, Yu Liu, Heekwon Lee, Xiao Huan, Shien-Ping Feng, Ho Cheung Shum, Barbara Pui Chan, Seung Kwon Seol, Jaeyeon Pyo,* and Ji Tae Kim*

Cite This: *Nano Lett.* 2021, 21, 5186−5194 Read Online

ACCESS | Metrics & More | Article Recommendations | Supporting Information

ABSTRACT: Hybrid perovskites are emerging as a promising, high-performance luminescent material; however, the technological challenges associated with generating high-resolution, free-form perovskite structures remain unresolved, limiting innovation in optoelectronic devices. Here, we report nanoscale three-dimensional (3D) printing of colored perovskite pixels with programmed dimensions, placements, and emission characteristics. Notably, a meniscus comprising femtoliters of ink is used to guide a highly confined, out-of-plane crystallization process, which generates 3D red, green, and blue (RGB) perovskite nanopixels with ultrahigh integration density. We show that the 3D form of these nanopixels enhances their emission brightness without sacrificing their lateral resolution, thereby enabling the fabrication of high-resolution displays with improved brightness. Furthermore, 3D pixels can store and encode additional information into their vertical heights, providing multilevel security against counterfeiting. The proof-of-concept experiments demonstrate the potential of 3D printing to become a platform for the manufacture of smart, high-performance photonic devices without design restrictions.

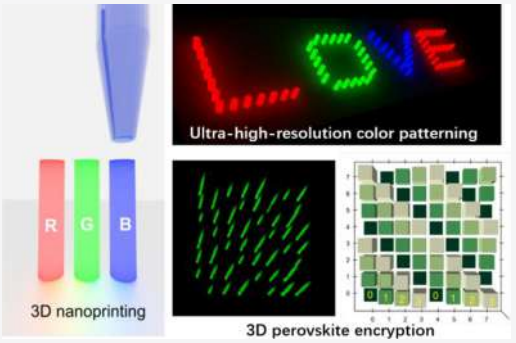

KEYWORDS: *3D printing, hybrid perovskite nanopixels, high-resolution displays, multilevel anticounterfeiting*

INTRODUCTION

A pixel is the smallest unit for displaying or storing information in the context of digital photonics, and there are continual demands for pixels that are smaller,[1−6] brighter,[7−9] and smarter.[10−12] In addition, appropriate encryption and authentication techniques are required for guarding access to the data stored in pixels, as counterfeiting has emerged as a global problem.[13−15] Extensive research on material system and device architecture is currently underway to develop pixels that meet these requirements for use in advanced applications.[16−18]

Hybrid perovskites show excellent potential for full-color display applications, due to their strong,[19−21] tunable,[8,12,22−24] high-color-purity photo- and electroluminescence.[25−27] Furthermore, these excellent optoelectronic properties can be obtained at low cost, as hybrid perovskites mostly adopt a low-temperature solution process.[28] Satisfying both the performance and cost is not easy for other commonly used materials for display applications such as inorganic III−V semiconductors, colloidal quantum dots, and organic molecules/polymers. Well-defined fabrication techniques are crucial to such practical applications; for example, the excellent solution processability of hybrid perovskites enables direct printing of color pixels onto large-area substrates via inkjet or electrohydrodynamic jet methods.[29−31] The printed pixels, however, suffer from coarse spatial resolution, ranging from a few micrometers to a few tens of micrometers, much larger than the diffraction limit of their emitted light. More sophisticated methods, such as electron beam lithography,[32,33] photolithography,[34−36] and nanoimprinting,[37,38] have been used to prepare micro- and nanopatterns of perovskites.[39] However, these methods are limited to the production of low-aspect-ratio thin-film pixels, whose emission brightness will significantly decrease due to the reduction in size.[9,40,41] Although a few methods based on physical vapor deposition have been devised to produce out-of-plane perovskite structures, the technological challenges associated with the precise control of perovskite dimensions, placements, and chemical compositions remain unresolved.[42−44]

Here, we report nanoscale 3D printing of perovskite nanopixels with programmed dimensions, placements, and emission characteristics. Our scheme is the use of a femtoliter-meniscus-guided *in situ* crystallization for 3D printing, enabling ultrahigh-density fabrication of vertically freestanding red,

Received: March 29, 2021
Revised: June 9, 2021
Published: June 14, 2021

https://doi.org/10.1021/acs.nanolett.1c01261
Nano Lett. 2021, 21, 5186−5194

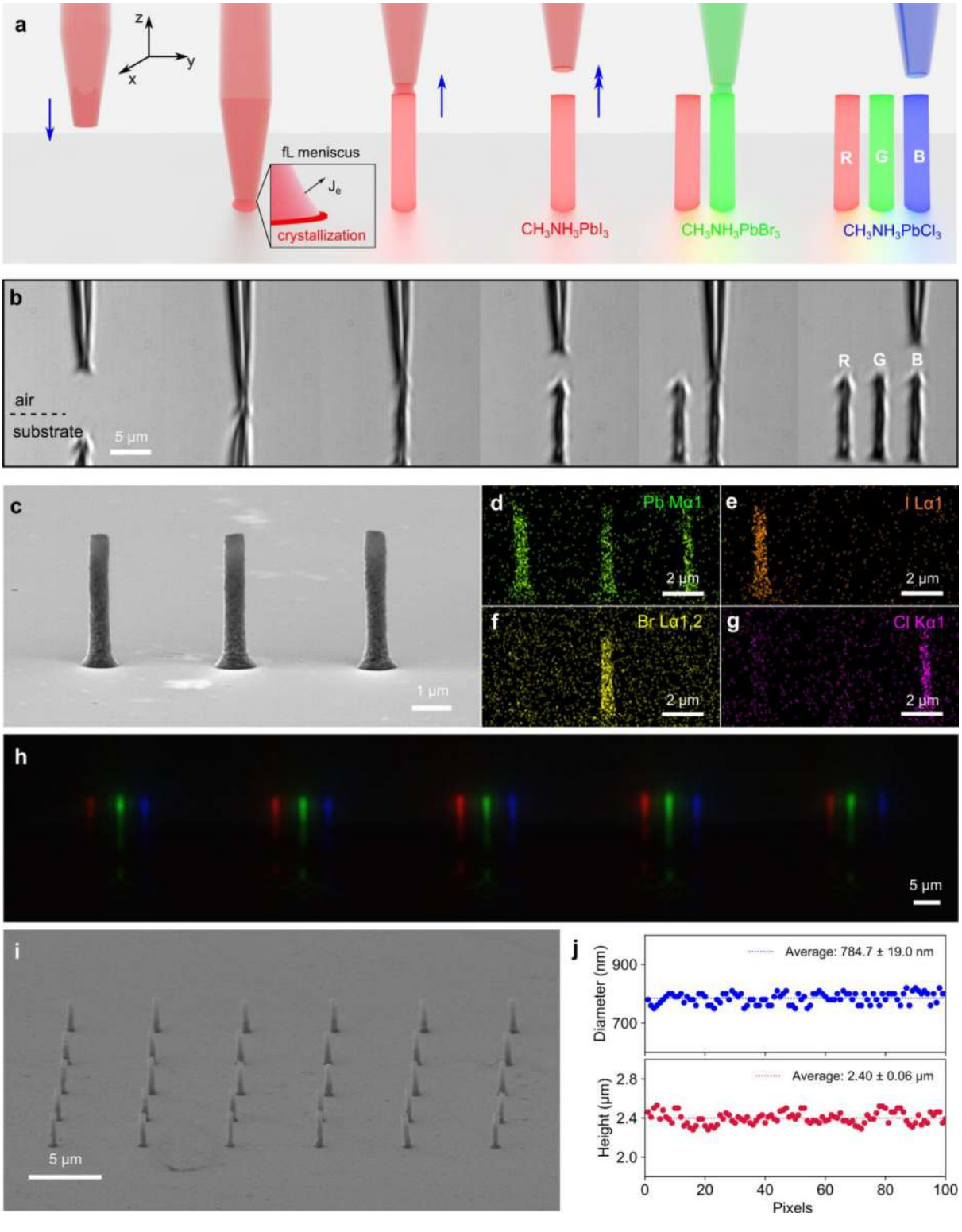

Figure 1. Three-dimensional (3D) printing of perovskite nanopixels. (a) Schematic showing the meniscus-guided crystallization process for the 3D printing of perovskites (fL = femtoliter). The process consists of (i) preparation of a nanopipet filled with a precursor ink, (ii) meniscus formation by pipet−substrate contact, (iii) meniscus-guided perovskite crystallization by upward movement of the pipet, and (iv) termination of crystallization by abruptly increasing the speed of pipet movement. This printing process can be used for different chemical compositions, enabling the fabrication of red (R), green (G), and blue (B) triple pixels. (b) Corresponding side-view real-time optical micrographs showing the printing process. (c) Field emission scanning electron microscopy (FE-SEM) image of an as-printed perovskite RGB triple pixel consisting of $CH_3NH_3PbI_3$ (R; left), $CH_3NH_3PbBr_3$ (G; middle), and $CH_3NH_3PbCl_3$ (B; right) nanopillars. (d−g) Corresponding energy dispersive X-ray spectroscopy images showing the chemical compositions of the tripixels: (d) lead, (e) iodide, (f) bromide, and (g) chloride. (h) Side-view optical photoluminescence image of an array of RGB tripixels. (i) FE-SEM image of an array of freestanding perovskite nanopillars. (j) Corresponding statistical data showing the printed diameter and height.

https://doi.org/10.1021/acs.nanolett.1c01261
Nano Lett. 2021, 21, 5186−5194

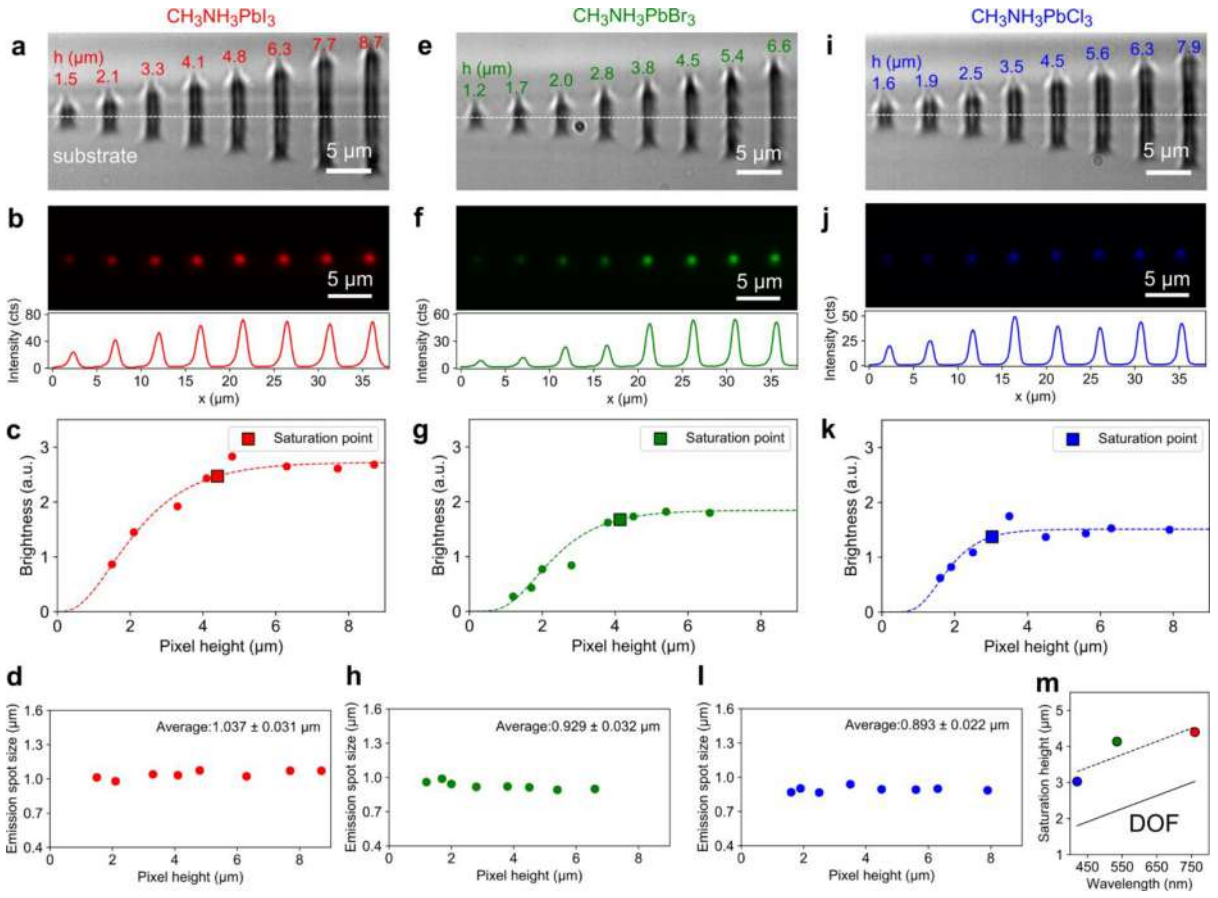

Figure 2. Pixel height, emission brightness, and spot size. (a–d) Three-dimensional-printed $CH_3NH_3PbI_3$ nanopixels (red) with controlled heights of 1.5, 2.1, 3.3, 4.1, 4.8, 6.3, 7.7, and 8.7 μm: (a) side-view optical micrograph, (b) bottom-view wide-field photoluminescence image (top) and its corresponding intensity profile (bottom), (c) emission intensity vs pixel height, and (d) emission spot size vs pixel height. (e–h) $CH_3NH_3PbBr_3$ (green) nanopixels and analysis corresponding to (a–d). (i–l) $CH_3NH_3PbCl_3$ (blue) nanopixels and quantitative analysis corresponding to (a–d). (m) Saturation height vs emission wavelength and its correlation with the depth of field (DOF).

green, and blue perovskite pixels with a lateral dimension of ~550 nm and a pitch ranging from 5 to 1.3 μm. Furthermore, the vertical on-demand printing process provides two key benefits. First, we show that increasing the pixel height can enhance emission brightness without decreasing the lateral resolution, which enables the formation of high-resolution display devices with improved brightness. Second, the pixel height can be used as an additional dimension in which to encode data, as it is not quantitatively accessible by conventional wide-field microscopes that are depth-of-field limited. Thus, by combining the luminescence of perovskite nanopixels with variations in pixel height, we demonstrate multilevel, high-resolution anticounterfeiting security labels. This work highlights the potential of 3D printing as a platform for the manufacture of smart, high-performance photonic devices.

RESULTS AND DISCUSSION

Figure 1a depicts the concept of our 3D perovskite printing approach. The key aspect that enables nanoscale 3D printing is the use of a meniscus comprising femtoliters of ink to confine and guide solution-mediated evaporation-driven crystallization in midair. To print red (R), green (G), and blue (B) nanopixels, the precursor inks are prepared by adding a methylammonium halide (CH_3NH_3I, CH_3NH_3Br, or CH_3NH_3Cl) and a lead halide (PbI_2, $PbBr_2$, or $PbCl_2$) into an *N*,*N*-dimethylformamide (DMF) and dimethyl sulfoxide (DMSO) mixture (1:1 volume ratio). First, at room temperature and 10% relative humidity, a glass nanopipet (diameter 600 nm; Figure S1 in the Supporting Information) filled with a precursor ink (e.g., a CH_3NH_3I and PbI_2 mixture for the generation of R-emitting pixels) is placed a few micrometers (μm) away from a silicon (Si) substrate. Then, the nanopipet and the substrate are physically contacted to form a femtoliter (fL)-volume meniscus of the precursor ink. Subsequent rapid evaporation of the solvent drives perovskite crystallization, leading to the formation of $CH_3NH_3PbI_3$ crystals inside the meniscus. Following the movement of the pipet with a constant speed of a few μm/s, the crystallization proceeds upward, which represents the 3D printing process. An abrupt increase in the speed at which the pipet moves terminates the printing process, producing a freestanding $CH_3NH_3PbI_3$ (R) nanopixel with the desired height (Figure S2 in the Supporting Information). The pixel diameter can also be controlled by varying the aperture diameter (Figure S3 in the Supporting Information) or moving speed of the pipet (Figure S4 in the Supporting Information).[45−49] Moreover, the use of different precursor inks, such as $CH_3NH_3Br/PbBr_2$ and $CH_3NH_3Cl/PbCl_2$, enables $CH_3NH_3PbBr_3$ (G) and $CH_3NH_3PbCl_3$ (B) nanopixels to be printed via the same protocol.

The entire printing process can be monitored in real time by side-view optical imaging, as shown in Figure 1b. The as-printed perovskite RGB nanopixels were examined by field emission scanning electron microscopy (FE-SEM). The FE-SEM image

https://doi.org/10.1021/acs.nanolett.1c01261
Nano Lett. 2021, 21, 5186−5194

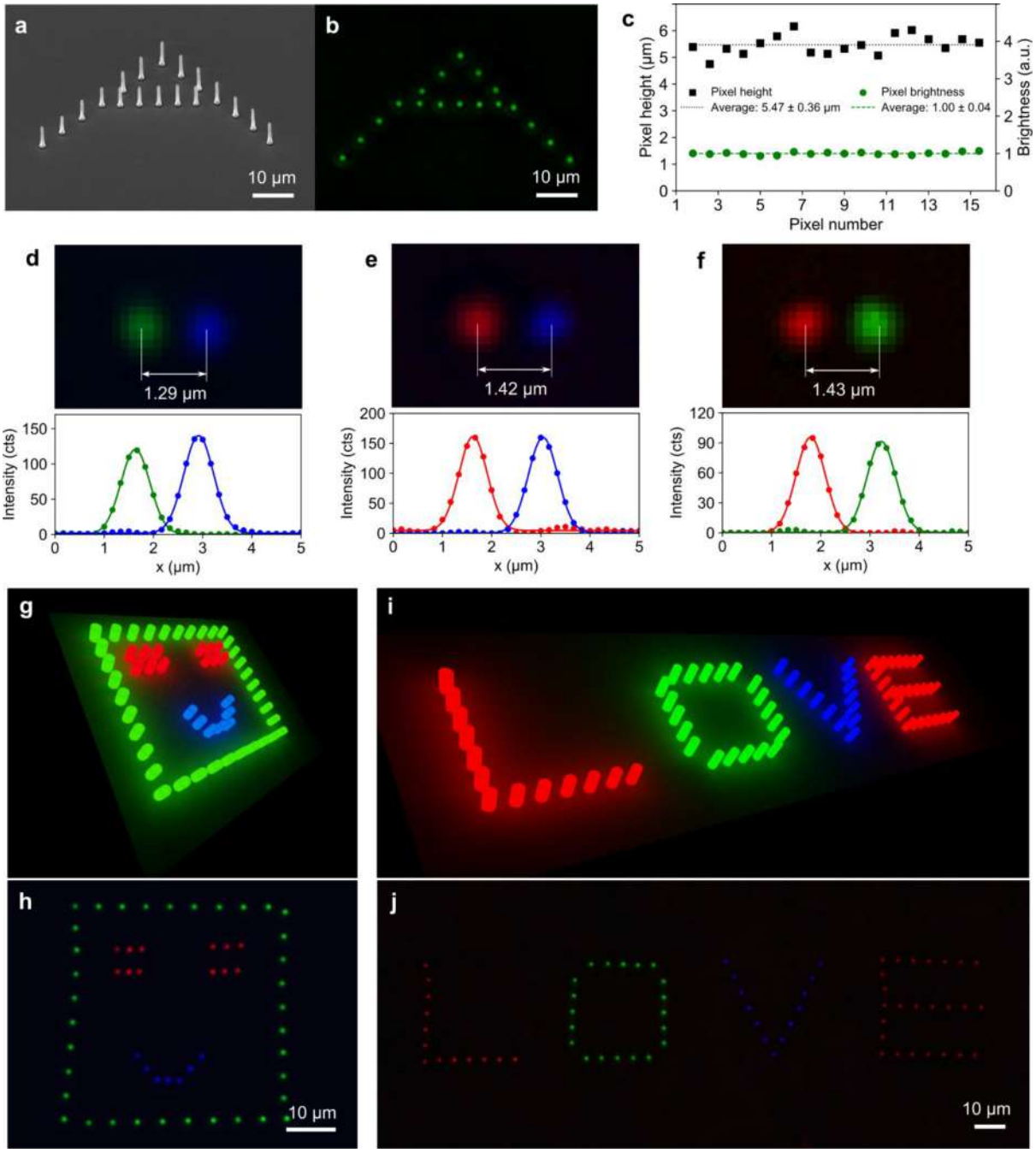

Figure 3. Bright nanopixel color displays. (a–c) 3D-printed "A"-shaped display: (a) 45° tilt-view FE-SEM image showing an "A"-shaped matrix consisting of vertical $CH_3NH_3PbBr_3$ nanopixels (green) with a height of ~5.47 ± 0.36 μm, (b) corresponding bottom-view PL image, and (c) quantitative distribution of the nanopixel height and brightness (au = arbitrary units). (d–f) Bottom-view PL images (top) and corresponding intensity profiles (bottom) of bicolor (d) G-B, (e) R-B, and (f) R-G nanopixels. (g–j) 3D-printed multicolor displays: (g) design scheme of a "smiley face" nanopixel matrix and (h) corresponding PL image and (i) design scheme of a nanopixel matrix spelling out "LOVE" and (j) corresponding PL image.

in Figure 1c shows an exemplary perovskite triple pixel consisting of $CH_3NH_3PbI_3$ (R; left), $CH_3NH_3PbBr_3$ (G; middle), and $CH_3NH_3PbCl_3$ (B; right) pillars with uniform dimensions (diameter 550 nm, height 4.1 μm) and a pitch of 5 μm. The chemical composition of this triple pixel was revealed by energy dispersive X-ray spectroscopy (EDS), as shown in Figures 1d–g. It can be seen that iodide (orange in Figure 1e), bromide (yellow in Figure 1f), and chloride (purple in Figure 1g) are well confined in the R, G, and B pillars, respectively, whereas lead (green in Figure 1d) is uniformly distributed over these three pillars. Figure 1h shows a side-view photoluminescence (PL) image of an array of perovskite RGB pixels under UV light illumination, with R, G, and B emissions visible through the radiative recombination of excitons (corresponding to emission peaks centered at 760, 535, and 420 nm, respectively, as shown in Figure S5 in the Supporting Information). The crystallographic information on the printed RGB nanopixels was obtained from transmission electron microscopy (TEM) and selected-area electron diffraction (SAED) measurements. Figure S6 confirms that the resulting

https://doi.org/10.1021/acs.nanolett.1c01261
Nano Lett. 2021, 21, 5186–5194

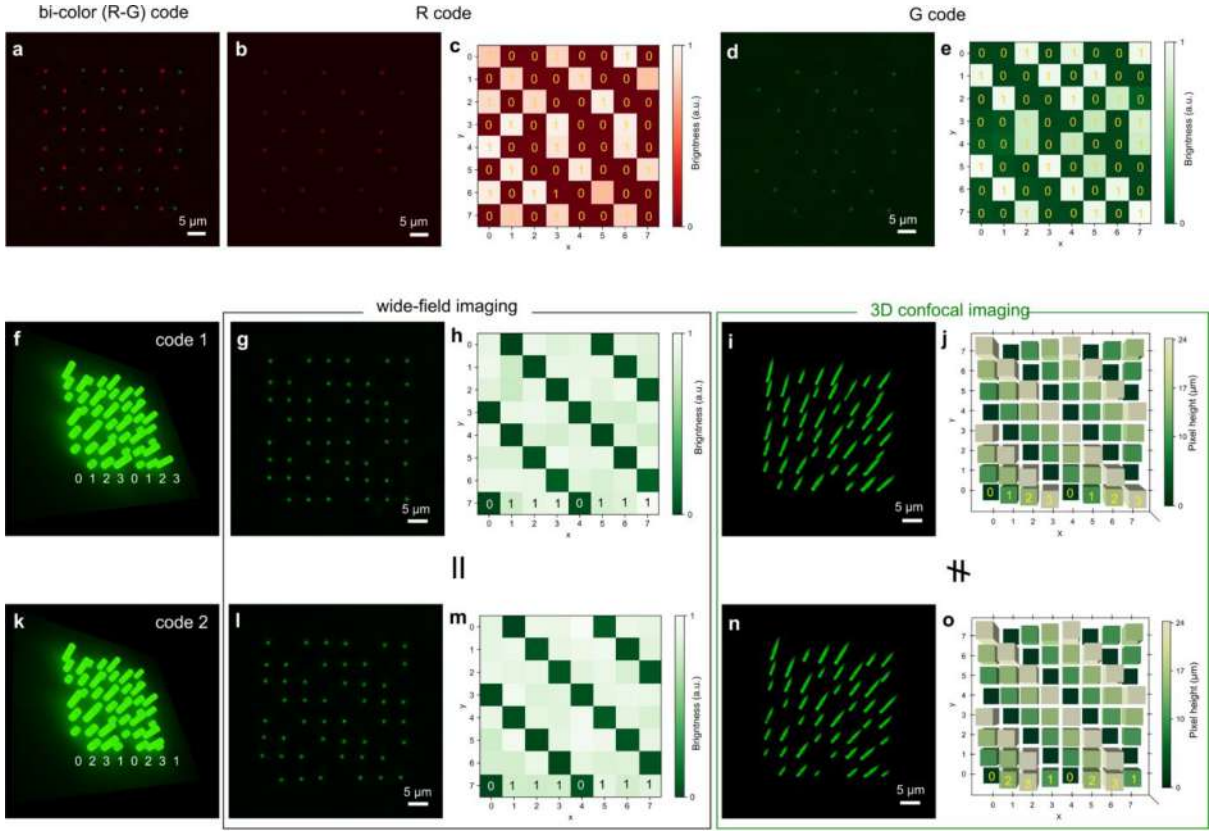

Figure 4. Multilevel anticounterfeiting. (a–e) Bicolor data matrix code: (a) bottom-view PL image of a bicolor code consisting of red (R) and green (G) 3D perovskite nanopixels, (b) PL image of an R code visualized using a R band-pass filter and (c) the corresponding binary information matrix, (d) PL image of a G code visualized using a G band-pass filter and (e) the corresponding binary information matrix. (f–j) Code 1, 2-bit, 8 × 8 3D matrix code consisting of G perovskite nanopixels with four different heights: (f) schematic design, (g) wide-field PL image of 3D-printed matrix code 1 and (h) the corresponding binary information, (i) 3D-printed code decrypted via 3D confocal PL imaging, and (j) decrypted 3D information. (k–o) code 2, where the first row encrypts "02310231," which is different from code 1: (k) schematic design, (l) wide-field PL image of the 3D-printed code 2, (m) the corresponding binary information, and (n) the corresponding 3D confocal PL image of the 3D-printed code 2 and (o) acquired 3D information.

RGB nanopixels exhibit polycrystallinity. Figure 1i,j shows that our perovskite printing process is reasonably reliable. The FE-SEM image in Figure 1i shows an array of freestanding nanopillars with a pitch of 5 μm. Figure 1j shows the statistical distribution of the measured diameters and heights of 100 nanopillars printed by the same protocol (printing speed 5 μm/s, termination speed 100 μm/s, and vertical displacement 2.4 μm; the FE-SEM images of these pillars are given in Figure S7 in the Supporting Information). These pillars have an average diameter of 780 nm, with a standard deviation of 19 nm (2.4%), and a height of 2.40 μm, with a standard deviation of 0.06 μm (2.5%). In addition, Figures S8 and S9 show the adhesion properties of the resulting pillars to the substrate withstanding substrate bending and compression, which are important characteristics for advanced flexible display applications.

The emission characteristics of the 3D-printed nanopixels were studied. Due to their small size, they are only visible under high-magnification imaging; thus, we investigated their emission intensity and size under UV excitation using a wide-field fluorescence microscope. A 40× objective lens (numerical aperture 0.55) was used to excite the pixels and collect their light emissions. The key benefit of 3D nanopixels is that their emission brightness can be varied in an on-demand fashion by adjusting their heights, without a concomitant decrease in the lateral resolution, as demonstrated in Figure 2. Figure 2a depicts a side-view optical image of printed $CH_3NH_3PbI_3$ nanopixels with an increasing range of heights (from 1.5 to 8.7 μm). Figure 2b shows the corresponding bottom-view wide-field PL image of these printed $CH_3NH_3PbI_3$ nanopixels and the intensity profile under UV excitation. The brightness of the nanopixels was quantified by the integration of the intensity counts in a bounded region around each nanopixel in the PL image. As can be seen in Figure 2c, the PL emission brightness of the nanopixels increases by ~3.3 times as their heights increase from 1.5 to 4.8 μm due to the increased pixel volume and its interaction with the excitation light. On the basis of this trend, we speculate that a pixel with a height of 4.8 μm may be ~24 times brighter than a 200 nm thick pixel (a typical thickness of a perovskite thin film; Figure S10 in the Supporting Information) with the same diameter.[26,27] As the height increases further from 4.8 to 8.7 μm, the emission brightness of the nanopixels remains constant, which indicates that they are saturated. The saturation height was determined to be 4.4 μm by fitting the brightness–height data with the Chapman–Richards growth function. This saturation of the collected PL emission may result from the limited depth of field (DOF) of the high-magnification wide-field imaging system. The light–matter interaction beyond the DOF does not contribute significantly to the collected emission brightness. Given that, we expect that it will be feasible to obtain a uniformly bright PL display by printing 3D nanopixels with heights greater than their saturation height.

https://doi.org/10.1021/acs.nanolett.1c01261
Nano Lett. 2021, 21, 5186–5194

Notably, the pixel height has a negligible effect on the size of the emission spot. Figure 2d shows the lateral emission sizes of nanopixels with different heights, which were measured from the full width at half-maximum of each emission peak (the corresponding Gaussian fit data are shown in Figure S11 in the Supporting Information). As was mentioned, despite the increase in pixel heights from 1.5 to 8.7 μm, the diameter of the emission spot remains constant, at 1.03 ± 0.03 μm. This result proves that our strategy can improve nanopixel brightness without sacrificing lateral integration density. Similar effects of pixel height on emission brightness and spot size are found for the colors obtained from $CH_3NH_3PbBr_3$ (G; Figure 2e,f and Figure S12 in the Supporting Information) and $CH_3NH_3PbCl_3$ (B; Figure 2i,j and Figure S13 in the Supporting Information) nanopixels. The emission brightness−height saturation curves and height-independent emission sizes of $CH_3NH_3PbBr_3$ (G; Figure 2g,h) and $CH_3NH_3PbCl_3$ (B; Figure 2k,l) pixels are also similar. Figure 2m shows the dependence of the saturation height on the emission wavelength: it can be seen that the saturation height increases from 3.0 to 4.4 μm as the emission wavelength increases from 420 to 760 nm. This linear trend (dashed line) may be caused by a linear DOF−wavelength dependence (solid line), as shown in the Supporting Information. The above findings demonstrate that our 3D printing approach enables exceptional on-demand controllability of nanopixel dimensions (height and diameter) at a single-entity level, which allows a flexible response to changes in the DOF of an optical imaging system.

Nanoscale 3D printing has the potential to produce ultrahigh-resolution color displays. In particular, the saturation behavior of nanoscale pixels (discussed in Figure 2) can be exploited to achieve uniform and highly intense emissions. The FE-SEM image in Figure 3a shows an "A"-shaped $CH_3NH_3PbBr_3$ nanopixel pattern with an average height of ∼5.4 μm (standard deviation 0.3 μm), which is greater than its saturation height (Figure 2g), fabricated on a quartz substrate. The corresponding PL image exhibits an "A"-shaped emission of uniform intensity (Figure 3b). Quantitative analysis results (Figure 3c) reveal that the emissions of these nanopixels exhibit only a 4% deviation resulting from their 6.6% height deviation. Figure 3d−f presents the bottom-view PL image and corresponding intensity profile of bicolor (G-B, R-B, and R-G) nanopixels with a pitch of <1.5 μm. Notably, our method provides a facile route to control the pitch down to ∼1.3 μm for high-density pixel integration (Figure S14 in the Supporting Information). Achieving a sub-micrometer pitch still remains a challenge in our printing configuration due to the unwanted merging between the feet of neighboring pixels. Designed multicolor displays with an ultrasmall (∼1 μm) emission spot and a micrometer pitch (<5 μm) are further demonstrated in Figure 3g−j. Figure 3g,h shows the design scheme and corresponding PL image of a "smiley face" comprising R, G, and B saturated nanopixels. In another example, the word "LOVE" is spelled out in three-color saturated nanopixels in Figure 3i,j.

We have also determined that these 3D-printed perovskite nanopixels can serve as building blocks for multilevel anticounterfeiting labels. The first level of security results from their small size; specifically, these sub-micrometer diameter nanopixels are invisible without the aid of a high-magnification microscope. A second level of security results from their fluorescent color information only being available upon UV excitation. Figure 4a shows a bicolor (R-G) data matrix code consisting of 3D-printed $CH_3NH_3PbI_3$ and $CH_3NH_3PbBr_3$ nanopixels visualized under a wide-field fluorescence microscope. The luminescent spots indicate "1", whereas the empty spots indicate "0". The selection of certain pixel colors allows two different binary information codes to be created. Thus, an R-G matrix code is shaped into a single-color R binary code via an R band-pass filter (Figure 4b), thereby decoding the selected binary information shown in Figure 4c. Analogously, a single-color G binary code is obtained via a G band-pass filter (Figures 4d,e).

The primary advantage of 3D-printed pixels is that they provide an additional dimension in which data can be stored and encrypted. For example, if an 8 × 8 matrix consists of pixels with four different heights, the resulting 2-bit, 8 × 8 matrix can encode 4^{64} combinations, which is far greater than the 2^{64} combinations that can be encoded by a binary 8 × 8 matrix. Figure 4f,k depicts the designs of two 3D matrix codes consisting of G perovskite nanopixels with four discrete heights of 0, 5, 10, and 15 μm, which are encoded as "0", "1", "2", and "3", respectively. We designed these two codes to have the same 2-bit configuration except in their first row, which is "01230123" for code 1 (Figure 4f) and "02310231" for code 2 (Figure 4k). Note that a wide-field fluorescence microscope is not able to access the entire information encoded in the nanopixel. As the pixel height of 5 μm for "1" is greater than the saturation height, the measured emission intensity presents only binary information. As a result, the PL images of codes 1 and 2 appear to be identical (Figure 4g,l). That is, their emission-intensity-based digital codes quantitatively exhibit the same information: e.g., the first rows of both codes denote "01110111" (Figure 4h,m). This demonstrates that height-encrypted 3D matrix codes have the same function as a binary Quick Response (QR) code. Furthermore, such height-encrypted 3D information can be decrypted via high-resolution 3D imaging: i.e., confocal microscopy. Thus, the confocal PL images of the 3D-printed codes 1 (Figure 4i) and 2 (Figure 4n) clearly show the 2-bit, 8 × 8 3D data matrix codes (Figure 4j,o, respectively), with their first rows denoting "01230123" and "02310231" separately, though the 2D information presents "01110111" identically, which proves that information can be encrypted within the pixel height to offer an additional level of security for anticounterfeiting applications. It is worth noting that the data-storage capacity and encryption level of these 3D-printed pixels can easily be enhanced by increasing the number of discrete height levels via our flexible and effective 3D printing strategy.

CONCLUSION

In conclusion, we have developed a nanoscale 3D printing method for fabricating perovskite-based RGB 3D nanopixels via femtoliter-meniscus-guided crystallization. This novel method enables facile, on-demand control of nanopixel emission brightness to be achieved by a precise tuning of pixel height, without a concomitant decrease in lateral resolution. Thus, these 3D nanopixels can be used to form ultrahigh-resolution and high-brightness displays. Moreover, we have demonstrated that the 3D pixel layout can be exploited to store and encrypt information for multilevel security labels that are inaccessible via wide-field imaging having a limited depth-of-field. This approach can be further improved by precise control of nanopixel dimensions, as can potentially be achieved by our 3D printing method. Our approach has the potential to diversify the nanopixel design with complex geometries, as demonstrated in Figure S15 in the Supporting Information, and the practicality could be advanced if the printing speed is improved. Our

https://doi.org/10.1021/acs.nanolett.1c01261
Nano Lett. 2021, 21, 5186−5194

recently developed parallel 3D printing[46] could be a viable solution to improve the printing speed and scalability of manufacturing. The new platform for perovskite 3D nanofabrication presented here opens up exciting new avenues for the realization of ultrahigh-resolution, multifunctional luminescent nanocrystal devices.

■ ASSOCIATED CONTENT

Supporting Information

The Supporting Information is available free of charge at https://pubs.acs.org/doi/10.1021/acs.nanolett.1c01261.

Experimental methods, theoretical calculation of DOF, FE-SEM image of a nanopipet used for nanoscale three-dimensional printing, high-aspect-ratio printing, 3D printing of nanopillars with different pipet sizes, printing diameter versus printing speed, normalized PL spectra of red (R), green (G), and blue (B) perovskite nanopixels, TEM characterization of perovskite nanopixels, FE-SEM images of 100 freestanding perovskite nanopillars, compression test of perovskite nanopillars, adhesion of perovskite nanopillars under substrate bending, difference in brightness between 2D dots and 3D saturated nanopillars, quantitative intensity analysis of arrayed $CH_3NH_3PbI_3$ nanopixels of increasing height, quantitative intensity analysis of arrayed $CH_3NH_3PbBr_3$ nanopixels of increasing height, quantitative intensity analysis of arrayed $CH_3NH_3PbCl_3$ nanopixels of increasing height, pitch control, and 3D-printed perovskites (PDF)

Meniscus-guided 3D printing of perovskite nanopixels (MOV)

Confocal PL imaging of the 3D-printed code 1 in Figure 4i (MOV)

Confocal PL imaging of the 3D-printed code 2 in Figure 4n (MOV)

Side-view optical imaging of the compression test of perovskite nanopillars (MOV)

■ AUTHOR INFORMATION

Corresponding Authors

Jaeyeon Pyo − *Nano Hybrid Technology Research Center, Korea Electrotechnology Research Institute (KERI), Changwon-si, Gyeongsangnam-do 51543, Republic of Korea;* orcid.org/0000-0002-8113-4232; Email: jpyo@keri.re.kr

Ji Tae Kim − *Department of Mechanical Engineering, The University of Hong Kong, Hong Kong, People's Republic of China;* orcid.org/0000-0003-4662-0179; Email: jtkim@hku.hk

Authors

Mojun Chen − *Department of Mechanical Engineering, The University of Hong Kong, Hong Kong, People's Republic of China*

Shiqi Hu − *Department of Mechanical Engineering, The University of Hong Kong, Hong Kong, People's Republic of China*

Zhiwen Zhou − *Department of Mechanical Engineering, The University of Hong Kong, Hong Kong, People's Republic of China*

Nan Huang − *Department of Mechanical Engineering, The University of Hong Kong, Hong Kong, People's Republic of China*

Sanghyeon Lee − *Department of Mechanical Engineering, The University of Hong Kong, Hong Kong, People's Republic of China*

Yage Zhang − *Department of Mechanical Engineering, The University of Hong Kong, Hong Kong, People's Republic of China;* orcid.org/0000-0002-1580-8200

Rui Cheng − *Department of Mechanical Engineering, The University of Hong Kong, Hong Kong, People's Republic of China*

Jihyuk Yang − *Department of Mechanical Engineering, The University of Hong Kong, Hong Kong, People's Republic of China*

Zhaoyi Xu − *Department of Mechanical Engineering, The University of Hong Kong, Hong Kong, People's Republic of China*

Yu Liu − *Department of Mechanical Engineering, The University of Hong Kong, Hong Kong, People's Republic of China*

Heekwon Lee − *Department of Mechanical Engineering, The University of Hong Kong, Hong Kong, People's Republic of China*

Xiao Huan − *Department of Mechanical Engineering, The University of Hong Kong, Hong Kong, People's Republic of China*

Shien-Ping Feng − *Department of Mechanical Engineering, The University of Hong Kong, Hong Kong, People's Republic of China;* orcid.org/0000-0002-3941-1363

Ho Cheung Shum − *Department of Mechanical Engineering, The University of Hong Kong, Hong Kong, People's Republic of China;* orcid.org/0000-0002-6365-8825

Barbara Pui Chan − *Department of Mechanical Engineering, The University of Hong Kong, Hong Kong, People's Republic of China;* orcid.org/0000-0001-5419-2472

Seung Kwon Seol − *Nano Hybrid Technology Research Center, Korea Electrotechnology Research Institute (KERI), Changwon-si, Gyeongsangnam-do 51543, Republic of Korea; Electrical-Functionality Materials Engineering, Korea University of Science and Technology (UST), Changwon-si, Gyeongsangnam-do 51543, Republic of Korea;* orcid.org/0000-0002-8733-4374

Complete contact information is available at: https://pubs.acs.org/10.1021/acs.nanolett.1c01261

Author Contributions

M.C. designed and performed the experiments and analyzed the data. S.H., S.L., J.Y., Z.X., Y.L., H.L., and S.K.S. contributed to the optimization of the 3D printing process. N.H. and B.P.C. contributed to the confocal imaging measurement. Z.Z., R.C., and S.-P.F. contributed to the preparation of perovskite inks. Y.Z. and H.C.S. contributed to the fluorescence imaging experiment. M.C., J.T.K., and J.P. wrote the manuscript. J.T.K. and J.P. supervised the project. All authors contributed to data analysis and have given approval to the final version of this manuscript.

Notes

The authors declare no competing financial interest.

■ ACKNOWLEDGMENTS

This work was supported by the Early Career Scheme (27207517) and the General Research Fund (17208218, 17208919, 17204020, 17128518) of the Research Grants Council of Hong Kong, the Environment and Conservation Fund (ECF 66/2018) of the HKSAR government, ITC Tier 3

(ITS-408-18), Innovation and Technology Fund, Innovation and Technology Commission, the Seed Fund for Basic Research (201910159047, 11159131) and Platform Technology Fund (102009742) of the University Research Committee (URC), The University of Hong Kong, and the Korea Electrotechnology Research Institute (KERI) Primary research program (21A01020) through the National Research Council of Science & Technology (NST) funded by the Ministry of Science and ICT.

REFERENCES

(1) Kumar, K.; Duan, H.; Hegde, R. S.; Koh, S. C. W.; Wei, J. N.; Yang, J. K. W. Printing Colour at the Optical Diffraction Limit. *Nat. Nanotechnol.* **2012**, *7*, 557−561.
(2) Zhu, X.; Vannahme, C.; Højlund-Nielsen, E.; Mortensen, N. A.; Kristensen, A. Plasmonic Color Laser Printing. *Nat. Nanotechnol.* **2016**, *11*, 325−329.
(3) Franklin, D.; Frank, R.; Wu, S.-T.; Chanda, D. Actively Addressed Single Pixel Full-Colour Plasmonic Display. *Nat. Commun.* **2017**, *8*, 15209.
(4) Su, M.; Huang, Z.; Li, Y.; Qian, X.; Li, Z.; Hu, X.; Pan, Q.; Li, F.; Li, L.; Song, Y. A 3D Self-Shaping Strategy for Nanoresolution Multicomponent Architectures. *Adv. Mater.* **2018**, *30*, 1703963.
(5) Li, Q.; Ji, M. G.; Kim, J. Grayscale Nanopixel Printing at Sub-10-nanometer Vertical Resolution via Light-Controlled Nanocapillarity. *ACS Nano* **2020**, *14*, 6058−6066.
(6) Ko, J.; Ma, K.; Joung, J. F.; Park, S.; Bang, J. Ligand-Assisted Direct Photolithography of Perovskite Nanocrystals Encapsulated with Multifunctional Polymer Ligands for Stable, Full-Colored, High-Resolution Displays. *Nano Lett.* **2021**, *21*, 2288−2295.
(7) Kwak, J.; Bae, W. K.; Lee, D.; Park, I.; Lim, J.; Park, M.; Cho, H.; Woo, H.; Yoon, D. Y.; Char, K.; Lee, S.; Lee, C. Bright and Efficient Full-Color Colloidal Quantum Dot Light-Emitting Diodes Using an Inverted Device Structure. *Nano Lett.* **2012**, *12*, 2362−2366.
(8) Zhang, F.; Zhong, H.; Chen, C.; Wu, X.-G.; Hu, X.; Huang, H.; Han, J.; Zou, B.; Dong, Y. Brightly Luminescent and Color-Tunable Colloidal $CH_3NH_3PbX_3$ (X = Br, I, Cl) Quantum Dots: Potential Alternatives for Display Technology. *ACS Nano* **2015**, *9*, 4533−4542.
(9) Bae, J.; Lee, S.; Ahn, J.; Kim, J. H.; Wajahat, M.; Chang, W. S.; Yoon, S.-Y.; Kim, J. T.; Seol, S. K.; Pyo, J. 3D-Printed Quantum Dot Nanopixels. *ACS Nano* **2020**, *14*, 10993−11001.
(10) Sun, B.; Edgar, M. P.; Bowman, R.; Vittert, L. E.; Welsh, S.; Bowman, A.; Padgett, M. J. 3D Computational Imaging with Single-Pixel Detectors. *Science* **2013**, *340*, 844−847.
(11) Phillips, D. B.; Sun, M.-J.; Taylor, J. M.; Edgar, M. P.; Barnett, S. M.; Gibson, G. M.; Padgett, M. J. Adaptive Foveated Single-Pixel Imaging with Dynamic Supersampling. *Sci. Adv.* **2017**, *3*, e1601782.
(12) Gao, Y.; Huang, C.; Hao, C.; Sun, S.; Zhang, L.; Zhang, C.; Duan, Z.; Wang, K.; Jin, Z.; Zhang, N.; Kildishev, A. V.; Qiu, C.-W.; Song, Q.; Xiao, S. Lead Halide Perovskite Nanostructures for Dynamic Color Display. *ACS Nano* **2018**, *12*, 8847−8854.
(13) Carro-Temboury, M. R.; Arppe, R.; Vosch, T.; Sørensen, T. J. An Optical Authentication System Based on Imaging of Excitation-Selected Lanthanide Luminescence. *Sci. Adv.* **2018**, *4*, e1701384.
(14) Tan, M.; Li, F.; Wang, X.; Fan, R.; Chen, G. Temporal Multilevel Luminescence Anticounterfeiting through Scattering Media. *ACS Nano* **2020**, *14*, 6532−6538.
(15) Zang, X.; Dong, F.; Yue, F.; Zhang, C.; Xu, L.; Song, Z.; Chen, M.; Chen, P.-Y.; Buller, G. S.; Zhu, Y.; Zhuang, S.; Chu, W.; Zhang, S.; Chen, X. Polarization Encoded Color Image Embedded in a Dielectric Metasurface. *Adv. Mater.* **2018**, *30*, 1707499.
(16) Liu, Y.; Han, F.; Li, F.; Zhao, Y.; Chen, M.; Xu, Z.; Zheng, X.; Hu, H.; Yao, J.; Guo, T.; Lin, W.; Zheng, Y.; You, B.; Liu, P.; Li, Y.; Qian, L. Inkjet-Printed Unclonable Quantum Dot Fluorescent Anti-Counterfeiting Labels with Artificial Intelligence Authentication. *Nat. Commun.* **2019**, *10*, 2409.
(17) Ren, W.; Lin, G.; Clarke, C.; Zhou, J.; Jin, D. Optical Nanomaterials and Enabling Technologies for High-Security-Level Anticounterfeiting. *Adv. Mater.* **2020**, *32*, 1901430.
(18) Deng, J.; Deng, L.; Guan, Z.; Tao, J.; Li, G.; Li, Z.; Li, Z.; Yu, S.; Zheng, G. Multiplexed Anticounterfeiting Meta-image Displays with Single-Sized Nanostructures. *Nano Lett.* **2020**, *20*, 1830−1838.
(19) Protesescu, L.; Yakunin, S.; Bodnarchuk, M. I.; Krieg, F.; Caputo, R.; Hendon, C. H.; Yang, R. X.; Walsh, A.; Kovalenko, M. V. Nanocrystals of Cesium Lead Halide Perovskites ($CsPbX_3$, X = Cl, Br, and I): Novel Optoelectronic Materials Showing Bright Emission with Wide Color Gamut. *Nano Lett.* **2015**, *15*, 3692−3696.
(20) Miao, Y.; Ke, Y.; Wang, N.; Zou, W.; Xu, M.; Cao, Y.; Sun, Y.; Yang, R.; Wang, Y.; Tong, Y.; Xu, W.; Zhang, L.; Li, R.; Li, J.; He, H.; Jin, Y.; Gao, F.; Huang, W.; Wang, J. Stable and Bright Formamidinium-Based Perovskite Light-Emitting Diodes with High Energy Conversion Efficiency. *Nat. Commun.* **2019**, *10*, 3624.
(21) Lu, M.; Guo, J.; Sun, S.; Lu, P.; Wu, J.; Wang, Y.; Kershaw, S. V.; Yu, W. W.; Rogach, A. L.; Zhang, Y. Bright CsPbI3 Perovskite Quantum Dot Light-Emitting Diodes with Top-Emitting Structure and a Low Efficiency Roll-Off Realized by Applying Zirconium Acetylacetonate Surface Modification. *Nano Lett.* **2020**, *20*, 2829−2836.
(22) Xing, G.; Mathews, N.; Lim, S. S.; Yantara, N.; Liu, X.; Sabba, D.; Grätzel, M.; Mhaisalkar, S.; Sum, T. C. Low-Temperature Solution-Processed Wavelength-Tunable Perovskites for Lasing. *Nat. Mater.* **2014**, *13*, 476−480.
(23) Fu, Y.; Zhu, H.; Stoumpos, C. C.; Ding, Q.; Wang, J.; Kanatzidis, M. G.; Zhu, X.; Jin, S. Broad Wavelength Tunable Robust Lasing from Single-Crystal Nanowires of Cesium Lead Halide Perovskites ($CsPbX_3$, X = Cl, Br, I). *ACS Nano* **2016**, *10*, 7963−7972.
(24) Xing, J.; Liu, X. F.; Zhang, Q.; Ha, S. T.; Yuan, Y. W.; Shen, C.; Sum, T. C.; Xiong, Q. Vapor Phase Synthesis of Organometal Halide Perovskite Nanowires for Tunable Room-Temperature Nanolasers. *Nano Lett.* **2015**, *15*, 4571−4577.
(25) Kojima, A.; Teshima, K.; Shirai, Y.; Miyasaka, T. Organometal Halide Perovskites as Visible-Light Sensitizers for Photovoltaic Cells. *J. Am. Chem. Soc.* **2009**, *131*, 6050−6051.
(26) Green, M. A.; Ho-Baillie, A.; Snaith, H. J. The Emergence of Perovskite Solar Cells. *Nat. Photonics* **2014**, *8*, 506−514.
(27) Yang, W. S.; Park, B.-W.; Jung, E. H.; Jeon, N. J.; Kim, Y. C.; Lee, D. U.; Shin, S. S.; Seo, J.; Kim, E. K.; Noh, J. H.; Seok, S. I. Iodide Management in Formamidinium-Lead-Halide-Based Perovskite Layers for Efficient Solar Cells. *Science* **2017**, *356*, 1376−1379.
(28) Veldhuis, S. A.; Boix, P. P.; Yantara, N.; Li, M.; Sum, T. C.; Mathews, N.; Mhaisalkar, S. G. Perovskite Materials for Light-Emitting Diodes and Lasers. *Adv. Mater.* **2016**, *28*, 6804−6834.
(29) Zhu, M.; Duan, Y.; Liu, N.; Li, H.; Li, J.; Du, P.; Tan, Z.; Niu, G.; Gao, L.; Huang, Y.; Yin, Z.; Tang, J. Electrohydrodynamically Printed High-Resolution Full-Color Hybrid Perovskites. *Adv. Funct. Mater.* **2019**, *29*, 1903294.
(30) Liu, Y.; Li, F.; Qiu, L.; Yang, K.; Li, Q.; Zheng, X.; Hu, H.; Guo, T.; Wu, C.; Kim, T. W. Fluorescent Microarrays of In Situ Crystallized Perovskite Nanocomposites Fabricated for Patterned Applications by Using Inkjet Printing. *ACS Nano* **2019**, *13*, 2042−2049.
(31) Shi, L.; Meng, L.; Jiang, F.; Ge, Y.; Li, F.; Wu, X.; Zhong, H. In Situ Inkjet Printing Strategy for Fabricating Perovskite Quantum Dot Patterns. *Adv. Funct. Mater.* **2019**, *29*, 1903648.
(32) Zhang, N.; Sun, W.; Rodrigues, S. P.; Wang, K.; Gu, Z.; Wang, S.; Cai, W.; Xiao, S.; Song, Q. Highly Reproducible Organometallic Halide Perovskite Microdevices based on Top-Down Lithography. *Adv. Mater.* **2017**, *29*, 1606205.
(33) Wang, S.; Liu, Y.; Li, G.; Zhang, J.; Zhang, N.; Xiao, S.; Song, Q. Lead Halide Perovskite Based Microdisk Lasers for On-Chip Integrated Photonic Circuits. *Adv. Opt. Mater.* **2018**, *6*, 1701266.
(34) Lyashenko, D.; Perez, A.; Zakhidov, A. High-Resolution Patterning of Organohalide Lead Perovskite Pixels for Photodetectors Using Orthogonal Photolithography. *Phys. Status Solidi A* **2017**, *214*, 1600302.

https://doi.org/10.1021/acs.nanolett.1c01261
Nano Lett. 2021, 21, 5186−5194

(35) Harwell, J.; Burch, J.; Fikouras, A.; Gather, M. C.; Falco, A. D.; Samuel, I. D. W. Patterning Multicolor Hybrid Perovskite Films via Top-Down Lithography. *ACS Nano* **2019**, *13*, 3823−3829.
(36) Xing, D.; Lin, C.-C.; Ho, Y.-L.; Kamal, A. S. A.; Wang, I.-T.; Chen, C.-C.; Wen, C.-Y.; Chen, C.-W.; Delaunay, J.-J. Self-Healing Lithographic Patterning of Perovskite Nanocrystals for Large-Area Single-Mode Laser Array. *Adv. Funct. Mater.* **2021**, *31*, 2006283.
(37) Wang, H.; Haroldson, R.; Balachandran, B.; Zakhidov, A.; Sohal, S.; Chan, J. Y.; Zakhidov, A.; Hu, W. Nanoimprinted Perovskite Nanograting Photodetector with Improved Efficiency. *ACS Nano* **2016**, *10*, 10921−10928.
(38) Li, Z.; Moon, J.; Gharajeh, A.; Haroldson, R.; Hawkins, R.; Hu, W.; Zakhidov, A.; Gu, Q. Room-Temperature Continuous-Wave Operation of Organometal Halide Perovskite Lasers. *ACS Nano* **2018**, *12*, 10968−10976.
(39) Jeong, B.; Han, H.; Park, C. Micro- and Nanopatterning of Halide Perovskites where Crystal Engineering for Emerging Photoelectronics Meets Integrated Device Array Technology. *Adv. Mater.* **2020**, *32*, 2000597.
(40) Kim, B. H.; Onses, M. S.; Lim, J. B.; Nam, S.; Oh, N.; Kim, H.; Yu, K. J.; Lee, J. W.; Kim, J.-H.; Kang, S.-K.; Lee, C. H.; Lee, J.; Shin, J. H.; Kim, N. H.; Leal, C.; Shim, M.; Rogers, J. A. High-Resolution Patterns of Quantum Dots Formed by Electrohydrodynamic Jet Printing for Light-Emitting Diodes. *Nano Lett.* **2015**, *15*, 969−973.
(41) Richner, P.; Galliker, P.; Lendenmann, T.; Kress, S. J. P.; Kim, D. K.; Norris, D. J.; Poulikakos, D. Full-Spectrum Flexible Color Printing at the Diffraction Limit. *ACS Photonics* **2016**, *3*, 754−757.
(42) Xing, J.; Liu, X. F.; Zhang, Q.; Ha, S. T.; Yuan, Y. W.; Shen, C.; Sum, T. C.; Xiong, Q. Vapor Phase Synthesis of Organometal Halide Perovskite Nanowires for Tunable Room-Temperature Nanolasers. *Nano Lett.* **2015**, *15*, 4571−4577.
(43) Chen, J.; Fu, Y.; Samad, L.; Dang, L.; Zhao, Y.; Shen, S.; Guo, L.; Jin, S. Vapor-Phase Epitaxial Growth of Aligned Nanowire Networks of Cesium Lead Halide Perovskites ($CsPbX_3$, X = Cl, Br, I). *Nano Lett.* **2017**, *17*, 460−466.
(44) Hu, X.; Zhou, H.; Jiang, Z.; Wang, X.; Yuan, S.; Lan, J.; Fu, Y.; Zhang, X.; Zheng, W.; Wang, X.; Zhu, X.; Liao, L.; Xu, G.; Jin, S.; Pan, A. Direct Vapor Growth of Perovskite $CsPbBr_3$ Nanoplate Electroluminescence Devices. *ACS Nano* **2017**, *11*, 9869−9876.
(45) Chen, M.; Yang, J.; Wang, Z.; Xu, Z.; Lee, H.; Lee, H.; Zhou, Z.; Feng, S.-P.; Lee, S.; Pyo, J.; Seol, S. K.; Ki, D.-K.; Kim, J. T. 3D Nanoprinting of Perovskites. *Adv. Mater.* **2019**, *31*, 1904073.
(46) Chen, M.; Xu, Z.; Kim, J. H.; Seol, S. K.; Kim, J. T. Meniscus-On-Demand Parallel 3D Nanoprinting. *ACS Nano* **2018**, *12*, 4172−4177.
(47) Kim, J. T.; Seol, S. K.; Pyo, J.; Lee, J. S.; Je, J. H.; Margaritondo, G. Three-Dimensional Writing of Conducting Polymer Nanowire Arrays by Meniscus-Guided Polymerization. *Adv. Mater.* **2011**, *23*, 1968−1970.
(48) Hu, J.; Yu, M.-F. Meniscus-Confined Three-Dimensional Electrodeposition for Direct Writing of Wire Bonds. *Science* **2010**, *329*, 313−316.
(49) Yi, Z.; Guo, J.; Chen, Y.; Zhang, H.; Zhang, S.; Xu, G.; Yu, M.; Cui, P. Vertical, Capacitive Microelectromechanical Switches Produced via Direct Writing of Copper Wires. *Microsyst. Nanoeng.* **2016**, *2*, 16010.

https://doi.org/10.1021/acs.nanolett.1c01261
Nano Lett. 2021, 21, 5186−5194